LUND UNIVERSITY

Remarkable variability in morphology, hygroscopicity and optical properties of soot aerosols during internal mixing in the atmosphere.

Zhang, Renyi Y; Khalizov, AF; Pagels, Joakim; Zhang, DD; Xue, H; McMurry, PH

Link to publication

Variability in morphology, hygroscopicity, and optical properties of soot aerosols during atmospheric processing

Renyi Zhang*†, Alexei F. Khalizov*, Joakim Pagels‡§, Dan Zhang*, Huaxin Xue*, and Peter H. McMurry‡

*Department of Atmospheric Sciences, Texas A&M University, College Station, TX 77843; ‡Department of Mechanical Engineering, University of Minnesota, Minneapolis, MN 55455; and §Division of Aerosol Technology, Ergonomics and Aerosol Technology, SE-211 00 Lund, Sweden

The atmospheric effects of soot aerosols include interference with radiative transfer, visibility impairment, and alteration of cloud formation and are highly sensitive to the manner by which soot is internally mixed with other aerosol constituents. We present experimental studies to show that soot particles acquire a large mass fraction of sulfuric acid during atmospheric aging, considerably altering their properties. Soot particles exposed to subsaturated sulfuric acid vapor exhibit a marked change in morphology, characterized by a decreased mobility-based diameter but an increased fractal dimension and effective density. These particles experience large hygroscopic size and mass growth at subsaturated conditions (<90% relative humidity) and act efficiently as cloud-condensation nuclei. Coating with sulfuric acid and subsequent hygroscopic growth enhance the optical properties of soot aerosols, increasing scattering by ≈10-fold and absorption by nearly 2-fold at 80% relative humidity relative to fresh particles. In addition, condensation of sulfuric acid is shown to occur at a similar rate on ambient aerosols of various types of a given mobility size, regardless of their chemical compositions and microphysical structures. Representing an important mechanism of atmospheric aging, internal mixing of soot with sulfuric acid has profound implications on visibility, human health, and direct and indirect climate forcing.

climate | clouds | radiative properties | human health | anthropogenic pollution

Soot aerosols produced from fossil-fuel combustion, automobile and aircraft emissions, and biomass burning are ubiquitous in the atmosphere, comprising ≈10–50% of the total tropospheric particulate matter (1–6). Once emitted into the atmosphere, soot particles are subjected to several aging processes, including adsorption or condensation of gaseous species (7–9), coagulation with other preexisting aerosols, and oxidation (10–12). Model calculations have shown that, when associated with other nonabsorbing aerosol constituents (e.g., sulfate), soot seems more absorptive and exerts a higher positive direct radiative forcing, and the warming effect by soot nearly balances the net cooling effect of other anthropogenic aerosols (5, 13). Also, on the basis of mesoscale model simulations, absorption of solar radiation by internally mixed soot aerosols causes warming in the middle atmosphere and reduction in cloudiness over the tropics (4). The mixing state and associated physical, optical, and geometrical properties of soot particles are of critical importance in evaluating the effects of light-absorbing aerosols and improving climate predictions by using global climate models (GCMs). Current knowledge on such an issue is very limited for developing an accurate representation of soot particles in GCMs, leading to underestimation of climatic forcing (14).

Hygroscopic aerosols also act as cloud-condensation nuclei (CCN) that impact cloud formation and the lifetime and albedo of clouds (4, 6). Freshly generated soot particles exist in the form of aggregates composed of hydrophobic primary spherules. The irregular geometry and complex microstructure of soot aggre-

gates may provide active sites for deposition of water and other chemical species (15). Enhanced hydrophilicity associated with soot-aging processes has been experimentally observed, including condensation of gaseous organics (9), H_2SO_4-exposed single-carbon microspheres (8), oxidation by OH, O_3, and HNO_3 (10–12), or engine combustion (16–18). For example, Wyslouzil *et al.* (8) used a 125- to 150-μm porous carbon sphere to represent combustion soot particles in hygroscopicity investigation, and the exposure method involved overnight treatment of carbon spheres with hot liquid sulfuric acid (97 wt % H_2SO_4 at 140°C) or sulfuric acid vapor in a highly supersaturated condition (97 wt % H_2SO_4 at 124–140°C). Most of the previous studies found relatively small hygroscopic growth of soot below water saturation [i.e., relative humidity (RH) < 100%] on the basis of measured changes in the mobility size, which depends on particle physical dimensions and morphology. In addition, previous experimental studies examined the optical properties of soot with coating of organic carbon or water (19, 20).

To date, the mixing state and variations in optical and cloud-forming properties of soot particles due to internal mixing in the atmosphere remain highly uncertain, considerably hindering efforts to assess their impact on visibility, human health, and climate. In this article we present laboratory measurements of the size-resolved mixing state, hygroscopicity, and optical properties of flame soot particles exposed to subsaturated sulfuric acid vapor to mimic internal mixing in the atmosphere. By combining measurements of particle mobility size and mass, we draw fundamental conclusions of atmospheric processing on the properties and effects of soot aerosols.

Results and Discussion

Fresh soot particles displayed predominantly chain agglomerates (Fig. 1*a*), with the spherical primary particles of ≈15-nm diameter clearly discernible. The mobility sizes of the soot aggregates collected by using a low-pressure impactor ranged from 50 to 245 nm. Sulfuric acid coating on soot was evident for samples collected after exposure to H_2SO_4 vapor. The coated soot aggregates were surrounded by smaller droplets of sulfuric acid, produced by splattering when the agglomerates deposited on the transmission electron microscope (TEM) grid (Fig. 1*b*). Formation of an external sulfuric acid–soot mixture was precluded in our study, because nucleation of sulfuric acid was inhibited at low RH (<0.5%) (21). The TEM measurements also revealed a marked change in morphology of the particles: soot agglomer-
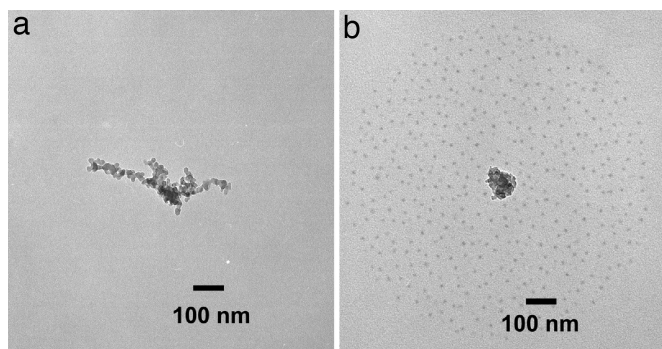
ENVIRONMENTAL SCIENCES

Fig. 1. TEM images of soot particles: fresh soot (*a*) and soot after exposure to H_2SO_4 vapor and 5% RH (*b*). The gaseous concentration of sulfuric acid is 1.4×10^{10} molecules·cm^{-3}. The cloud of small droplets surrounding the soot particle corresponds to sulfuric acid, which was shaken off the coated soot particle after impacting on the TEM grid. A high impacting velocity of soot particles on the grid surface resulted in a circular and uniform distribution of small sulfuric acid droplets around the soot core. The droplets gradually disappeared after exposure to heating produced by the electron beam as a result of evaporation, confirming their volatile nature. The particle concentrations were monitored upstream and downstream of the H_2SO_4 bath to confirm that particle concentrations did not increase as a result of particle nucleation.

ates after H_2SO_4 exposure exhibited a considerable restructuring and shrinking to a more compact form (Fig. 1*b*).

Because of the complex morphology of soot particles, we used two approaches to characterize the mixing state and hygroscopic growth on the basis of a particle mobility-based diameter ratio D_p/D_o and mass ratio m_p/m_o, where the subscripts p and o denote the H_2SO_4-coated (condensed) and fresh particles, respectively. There existed distinct patterns between the changes in the mobility diameter and mass of soot particles after exposure to gaseous H_2SO_4 (Fig. 2*a*). Measurements with a tandem differential mobility analyzer (TDMA) showed that the mobility diameter decreased after H_2SO_4 exposure, with the D_p/D_o value of slightly less than unity for 50-nm particles and 0.6 for 360-nm particles. In contrast, the particle mass measured by an aerosol particle mass (APM) analyzer increased after exposure to H_2SO_4 because of H_2SO_4 condensation to the soot particles. The H_2SO_4 mass fractions of the coated soot particles reached 0.43 for 50-nm particles and 0.35 for 360-nm particles. Combining the mobility diameter and mass measurements yielded the effective density, which changed from 0.56 to 1.60 g·cm^{-3} for 50-nm particles and from 0.10 to 0.94 g·cm^{-3} for 360-nm particles after H_2SO_4 condensation (Fig. 2*b*). The effective density of H_2SO_4-coated soot particles was $\approx$3–10 times larger than that for fresh soot agglomerates, reflecting soot restructuring and consistent with TEM measurements (Fig. 1). The compaction was more pronounced for larger soot agglomerates. The decrease in mobility diameter was also accompanied by a change in particle fractal dimension, which increased from 2.1 for fresh soot to 2.8 for H_2SO_4-coated soot exposed to 90% RH (Fig. 2*b*). The effective density and fractal dimension of H_2SO_4-coated soot approached the estimated bulk values (1.7 g·cm^{-3} and 3, respectively) of the soot–H_2SO_4 mixture, indicating a transformation from highly agglomerated to nearly spherical particles. Hence, although the measurements based on the particle mobility-equivalent diameter alone were inconclusive because of restructuring, the mixing state of soot particles could be quantified from the combined measurements of particle mobility size and mass. Other previous studies also found variable effective density and fractal dimension of soot particles from diesel combustion by using combined size and mass measurements (22, 23). We found that soot agglomerates subjected to H_2SO_4 condensation and

subsequent heating to 200°C recovered their initial mass (1.01 ± 0.04) despite changes in morphology (Fig. 2*b*), indicating negligible chemical interaction between sulfuric acid and the soot surface and a physical adsorption process. In a recent Fourier transform infrared spectroscopy study of soot particles exposed to sulfuric acid vapor (7), the observed spectral features were described as a superposition of soot and sulfuric acid spectra, showing no chemical interaction between soot particles and H_2SO_4.

The hygroscopic size (Fig. 2*c*) and mass (Fig. 2*d*) growths of both fresh and H_2SO_4-coated soot were measured at various fresh-particle diameters between 50 and 245 nm as a function of RH. For fresh soot of all sizes we found little change in the particle mobility size in the RH range of 5–90%, indicating negligible growth or shrinkage. Considerable change in the mobility size was observed for H_2SO_4-coated soot agglomerates. The hygroscopic size and mass growth depended on the initial fresh-particle size and RH (Figs. 2 *c* and *d*). The growth (size or mass) ratios were referred to H_2SO_4-coated soot particles at 5% RH (D_o or m_o). The size growth curve for 50-nm particles had a shape characteristic of pure H_2SO_4 droplets, but the maximum growth factor (1.52 at 90% RH) was less than that of pure sulfuric acid (2.03). Mobility sizes of larger particles, with diameters of 155 and 245 nm, decreased when RHs were increased to 20–50%, presumably because of collapse of the agglomerates that occurred after uptake of H_2SO_4 and H_2O. At 90% RH, however, the uptake was sufficient to produce significant growth in mobility sizes. The hygroscopic mass growth, however, increased steadily with RH for all particle sizes (Fig. 2*d*), indicating H_2O condensation and a net mass gain. The mobility-size growth factor showed a stronger dependence on the initial particle size than the mass growth factor for a given RH. The delayed and smaller hygroscopic size growth for larger soot particles was also indicative of restructuring after condensation of water. The smaller 50-nm soot agglomerates were sufficiently compact and acquired a larger H_2SO_4 mass fraction to cause nearly complete restructuring and subsequent growth at 5% RH. Larger, more agglomerated particles with a lower density and lower H_2SO_4 mass fraction exhibited growth only at a higher RH (20–50%) after substantial restructuring of the agglomerates.

The irregular geometry and complex microstructure of soot agglomerates have been suggested to enhance condensation of water and other chemical species because of a decreased equilibrium vapor pressure from the negative curvature (Kelvin) effect (15), especially for larger particles. We measured the absolute mass coating of sulfuric acid on soot agglomerates and polystyrene latex (PSL) spheres (Fig. 2*e*) to evaluate the effects of chemical composition and morphology. Soot is graphite-like and a highly conjugated polycyclic aromatic system, whereas PSL is a saturated polymer chain with aromatic substituents. The differences in the molecular composition between soot and PSL lead to distinct chemical and physical properties. For instance, soot is a strong light absorber and a good electrical conductor, whereas PSL is transparent and dielectric. Nevertheless, soot and PSL particles of similar mobility sizes acquired almost identical masses of sulfuric acid (Fig. 2*e*). The measurements between soot and PSL also provided a comparison for irregular aggregates and smooth spherical particles, indicating that the H_2SO_4 coating was independent of the chemical makeup and microphysical structure of the particles. The efficient H_2SO_4 coating on the two types of particles is explained by the sticky nature and high water affinity of H_2SO_4. Sulfuric acid molecules readily condense on particles, and the condensed H_2SO_4 is subsequently stabilized from the interaction with water vapor: water uptake onto the condensed H_2SO_4 lowers the equilibrium vapor pressures of both components (H_2SO_4 and water) and causes the condensation
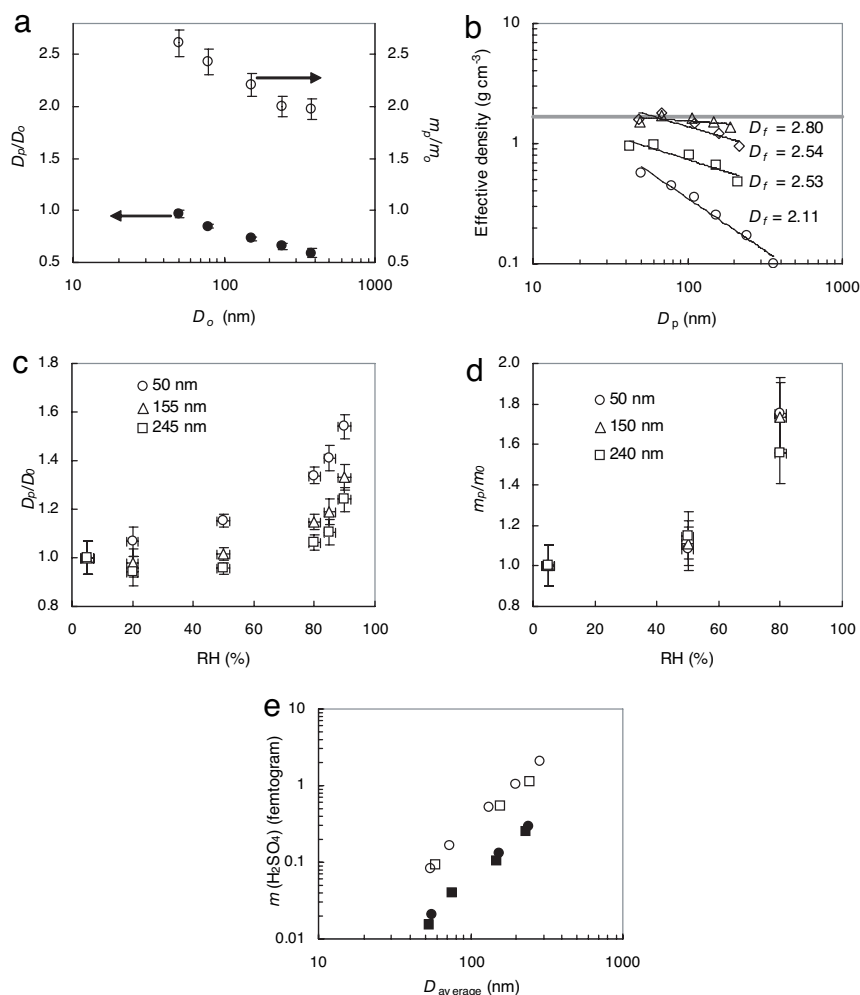
Fig. 2. Effects of sulfuric acid on properties of aerosol particles. (*a*) Changes in the particle mobility size and mass after exposure of soot agglomerates to sulfuric acid and water: the particle size D_p/D_o (filled circles and left axis) and mass m_p/m_o (open circles and right axis) ratios after H_2SO_4 exposure and H_2O stabilization at 5% RH. The gaseous concentration of sulfuric acid is 1.4×10^{10} molecules·cm^{-3}. The subscripts p and o refer to H_2SO_4-coated soot particles at 5% RH and fresh soot particles, respectively. (*b*) Effective density (ρ_{eff}) of fresh and exposed soot determined from the mass [differential mobility analyzer–aerosol particle mass (DMA–APM)] and mobility (DMA–DMA) measurements: circles, fresh soot; diamonds, H_2SO_4-coated soot at RH 5%; squares, H_2SO_4-coated soot heated to 200°C to remove condensed sulfuric acid; triangles, H_2SO_4-coated soot humidified to RH 90% and then dried to a RH of 5%. The gray line corresponds to the estimated bulk density of the soot–H_2SO_4 mixture (1.7 g·cm^{-3}). The H_2SO_4 concentration is 1.4×10^{10} molecules·cm^{-3}. The fractal dimension (D_f) is 2 for a plane and 3 for a solid sphere. (*c*) Hygroscopic mobility-size growth ratio (D_p/D_o) of H_2SO_4-coated soot particles. The H_2SO_4 concentration is 1.4×10^{10} molecules·cm^{-3}. The subscripts p and o refer to H_2SO_4-coated soot particles at a higher RH and at 5% RH, respectively. The circles, triangles, and squares correspond to coated soot particles with fresh-particle sizes of 50, 155, and 245 nm, respectively. (*d*) Hygroscopic mass growth ratio (m_p/m_o) of H_2SO_4-coated soot particles. The H_2SO_4 concentration is 1.4×10^{10} molecules·cm^{-3}. The subscripts p and o refer to H_2SO_4-coated soot particles at a higher RH and at 5% RH, respectively. The circles, triangles, and squares correspond to coated soot particles with fresh-particle sizes of 50, 155, and 245 nm, respectively. (*e*) Absolute-mass coating of sulfuric acid on soot agglomerates (squares) and PSL spheres (circles) after H_2SO_4 exposure and H_2O stabilization at 5% RH. Open and filled symbols represent sulfuric acid vapor concentrations of 1.4×10^{10} and 2.5×10^9 molecules·cm^{-3}, respectively. The diameter ($D_{average}$) corresponds to the average of uncoated and coated particle, because the mobility diameter varies after sulfuric acid condensation. In *a*, *c*, and *d*, the vertical error bars represent random error of the measurements (2 SDs), and the values are averaged over at least two measurements.

process to be practically irreversible under typical atmospheric conditions (24, 25).

Our measurements suggest that the condensation rate of sulfuric acid is proportional to the particle surface area regardless of the particle morphology. The surface area of soot agglomerates can be approximated by the surface area of a sphere of similar mobility diameter. To validate this assumption, we calculated the surface area of fresh soot agglomerates by using the absolute masses of soot agglomerates from DMA–APM measurements, the diameters of primary spheres from TEM photographs, and the material soot density of 1.77 g·cm^{-3}. Assuming that the surface area of agglomerates is represented as the sum of surfaces of primary spheres, we found that the surface

areas of fresh soot particles were close to the areas of solid spheres of the same mobility diameter. The dependence of the condensed H_2SO_4 mass varied closely with the square of mobility size, because the data in Fig. 2*e* could be expressed in the form of the condensed H_2SO_4 mass $\propto D_p^x$, and the proportionality factor was determined by the gaseous H_2SO_4 concentration. The power-law fit to the data presented in Fig. 2*e* produced excellent correlation ($r^2 = 0.99$) between the coated H_2SO_4 mass and the particle size with the exponent (x) in the range of 1.8–1.9. Our laboratory results are consistent with atmospheric measurements showing that the steady-state atmospheric H_2SO_4 concentrations are reasonably predicted from the production rates and loss rates by condensation on preexisting particles, if the loss
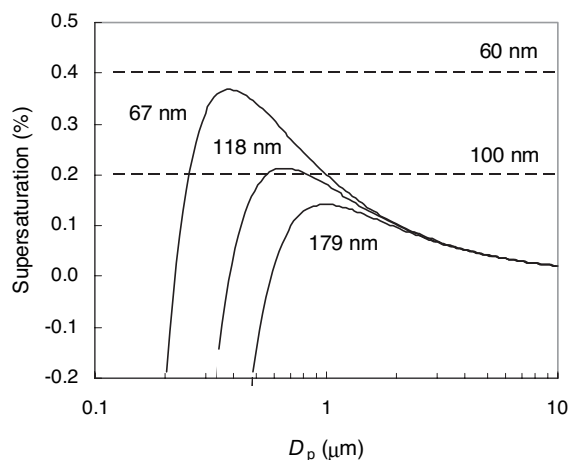
Fig. 3. Cloud-activation properties of soot particles coated with sulfuric acid. The activation was computed with Köhler theory by using hygroscopic growth factors measured at 90% RH for particles with D_o = 67, 118, and 179 nm. The dashed lines display the supersaturation at which coated soot particles with D_o = 60 and 100 nm activate into cloud droplets measured experimentally with a CCN counter.

Fig. 4. Extinction (σ_{ext}) (a), scattering (σ_{sca}) (b), and absorption-specific (σ_{abs}) (c) cross-sections of soot particles with a fresh mobility diameter of 320 nm. The filled and open symbols correspond to the optical properties of fresh and sulfuric acid-coated soot particles, respectively. The vertical error bars represent random error of the measurements (2 SDs), and the values are averaged over at least three measurements.

rate to preexisting particles is assumed to be diffusion-controlled with an accommodation coefficient of unity (26).

In our experiments, the flame soot was exposed to sulfuric acid vapor by passing through a H_2SO_4 reservoir at room temperature. The coated H_2SO_4 amount on soot particles was proportional to the exposure time, vapor concentration of H_2SO_4, and particle surface area (or particle size) (Fig. 2e). The residence time of the soot-laden flow in the reservoir was ≈10 sec, whereas the H_2SO_4 vapor concentration (10^9 to 10^{10} molecules·cm^{-3}) in the reservoir was higher than that in the atmosphere (10^4 to 10^8 molecules·cm^{-3}) (27). Assuming a typical daytime H_2SO_4 concentration of 10^7 molecules·cm^{-3}, we estimated that <5 h would be required to acquire an H_2SO_4 mass fraction of 0.35–0.45 for freshly emitted soot. This case likely corresponds to polluted conditions with emissions from power plants that contain large amounts of soot and SO_2. Even after exposure to sulfuric acid of 10^5 molecules·cm^{-3}, a period of ≈3 days is sufficient for soot particles to acquire ≈10% H_2SO_4 by mass and to become hygroscopic. Hence, the composition, mass, and morphology of soot aerosols will be considerably altered during their typical lifetimes of ≈1 week (13). Previous field measurements of the mixing state of soot revealed that freshly emitted soot particles are externally mixed, whereas aged soot particles are mostly mixed internally (28). It has also been shown that over a remote marine atmosphere almost all soot particles contained sulfate (29). It should be pointed out that condensation of organics onto soot particles may also occur in addition to that of H_2SO_4 in the atmosphere (30). However, it is likely that H_2SO_4 will have a much larger effect on processing of soot aerosols than organics, and condensation of H_2SO_4 largely determines the aerosol hygroscopicity. Also, H_2SO_4 condensed on aerosol particles may promote heterogeneous reactions of carbonyls and alcohols (31, 32).

We applied Köhler theory (33) to the measured hygroscopic growth factors to evaluate the ability of aged soot particles to serve as CCN. For the H_2SO_4-coated particles of 67–179 nm (at 5% RH), the critical supersaturation (S_c), defined as the peak supersaturation on the Köhler curve, was estimated to be in the range of 0.37–0.14% (Fig. 3), with smaller S_c values for larger particles. By using a CCN counter, the S_c values were measured directly as 0.4% and 0.2% for soot sizes of 60 and 100 nm, respectively, which is in agreement with the calculations. Under
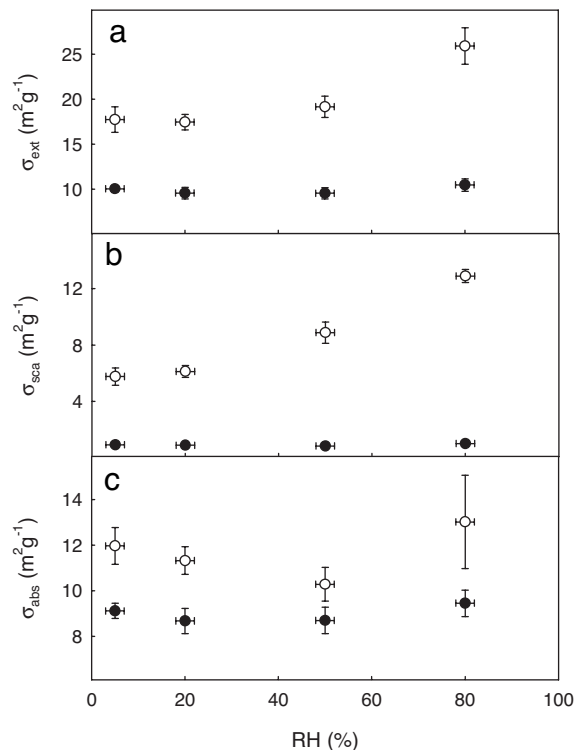
cloud conditions, aerosols with S_c values less than the ambient supersaturation activate to form cloud droplets. Atmospheric measurements indicated that cloud supersaturation reaches up to 2% in the troposphere (33). Hence, aged soot particles with H_2SO_4 coating activate readily under various cloud conditions.

To quantify the effect of the mixing state on optical properties of soot, we measured the extinction and scattering cross-sections of fresh and coated soot particles of 320-nm initial mobility diameter (Fig. 4). The measurements were performed at 532-nm wavelength and 5–80% RH. The light absorption was determined from the difference between light extinction and scattering. The optical properties of fresh soot particles were independent of RH below water saturation, which is in agreement with the hygroscopic measurements. The scattering and extinction cross-sections of fresh soot particles were 2.1×10^{-11} and 2.1×10^{-10} cm^2, respectively, with a single scattering albedo of ≈0.1. The specific absorption cross-section of fresh soot particles was determined to be 8.7 m^2·g^{-1}, which is in agreement with the orientation-averaged value of ≈6.6 m^2·g^{-1} calculated previously (34). Internal mixing of soot agglomerates with sulfuric acid resulted in a dramatic change in the optical properties even at 5% RH. Scattering by coated soot was enhanced by a factor of 5.5 at 5% RH relative to that of fresh soot. Despite their relatively large mobility size, fresh soot agglomerates showed weak scattering even when the fresh particles had a larger mobility diameter than the coated particles (in the case of 5% RH), which occurs because individual primary spherules in the agglomerates are loosely connected and act independently in light scattering. The formation of an aqueous shell and compaction of the soot core both contributed to the increase in scattering by coated soot particles. After internal mixing with H_2SO_4 and compaction of

aggregates, the primary spherules interact collectively with electromagnetic waves to lead to stronger scattering. Increasing RH resulted in further growth of the aqueous shell and scattering enhancement, reaching a factor of 10 at 80% RH. A similar yet smaller enhancement was observed for the absorption cross-section, which increased by a factor of 1.5 after H_2SO_4 coating and subsequent exposure to 80% RH. The absorption cross-section did not vary monotonically with RH because of the competition between water condensation and soot-core restructuring. A minimum in absorption cross-section at ≈50% RH likely corresponded to the nearly complete compaction of the soot agglomerates observed in TDMA measurements (Fig. 2c). At 80% RH, the scattering and extinction cross-sections of coated particles were 2.6×10^{-10} and 5.2×10^{-10} cm^2, yielding a single scattering albedo of 0.5. We observed similar but weaker optical effects for smaller soot particles, indicating that the optical effects were more pronounced for larger particles (i.e., 320 nm). The changes in the effective density and optical properties of coated soot also alter the effective refractive index, which is another factor that determines the optical properties. Previous calculations have suggested an increased absorption cross-section attributable to coating of inorganic salts on soot particles (5, 34) but could not to take into account the complex variation in morphology of soot agglomerates during atmospheric processing.

Our measurements provide quantitative determination of the mixing state, morphology, hygroscopicity, optical properties, and CCN activation of soot internally mixed with sulfuric acid. The results reveal that soot particles acquire a large mass fraction of sulfuric acid during atmospheric aging. Most previous studies found small hygroscopic growth of soot (with a size growth factor of <1.1) at 80% RH (8–12, 15–17). Because the coating of soot agglomerates with sulfuric acid and water is accompanied by restructuring to a more compact form, the measurement of mobility-size growth factors by using TDMA alone, a technique widely used in atmospheric field studies, may not accurately reflect the mixing state of soot particles or, thus, the hygroscopic properties. The changes in the morphology and effective density of soot aerosols during atmospheric processing are likely relevant to health effects such as deposition of particles in the human respiratory system (35). We also demonstrate that the condensation of H_2SO_4 occurs at a similar rate on soot agglomerates and PSL spheres of the same mobility size. Under typical tropospheric RH conditions, H_2SO_4 molecules will readily condense onto aerosol surfaces because of its sticky nature. Subsequently, the condensed H_2SO_4 will be effectively stabilized by water molecules, leading to irreversible condensation. The H_2SO_4 condensation rate will only depend on the particle surface area (and hence size) but is independent of morphology or chemical composition of aerosols. Hence, our observation is applicable to atmospheric particles of other types, and the results provide guidance for modeling mass transfer on atmospheric aerosols, which is essential to assessment of their atmospheric lifetimes and climate impacts.

The dramatic internal mixing and hygroscopic growth of soot particles under subsaturated conditions likely impact visibility and air quality, in addition to direct and indirect climate forcing. Our results imply that the aerosol optical depth (visibility) of aged soot in polluted air is considerably enhanced (decreased) compared with fresh soot and correlates strongly with RH. Enhanced light absorption and scattering caused by condensation of gaseous H_2SO_4 on soot particles can stabilize the atmosphere because of cooling at the surface and warming aloft. A stable atmosphere retards vertical transport (36), which will have an important feedback on air quality, because a stable atmosphere exacerbates accumulation of gaseous and particulate matter pollutants within the planetary boundary layer (PBL). For the local and regional climate, a large optical effect

of aged soot reduces the diurnal variation of the near-surface temperature, whereas trapping of water vapor within the PBL increases humidity near the surface. Less surface heating and atmospheric stabilization will also impact cloud dynamics by reducing vertical sensible and latent heat exchanges and restricting convective development (4, 36), whereas warming in the atmosphere will decrease RH or supersaturation (36). The exact radiative and cloud-forming effects of soot particles in the atmosphere will depend on the time scale of the aging process and the number fraction of the internally H_2SO_4-mixed soot particles in the total aerosol population. It is plausible that the optically induced effects of aged soot particles (i.e., atmospheric stabilization and decreasing RH or supersaturation) dominate under heavily polluted conditions (36), whereas the CCN effect is more pronounced in less polluted air or for transported particles in the regional and global atmosphere (37).

Methods

Soot particles were generated by incomplete combustion of propane in a Santoro-type laminar diffusion burner (7). Typical flow rates were 30 ml·min^{-1} of propane and 1.7 liter·min^{-1} of air. Soot particles were collected through a 0.5- to 1.0-mm orifice in a stainless steel sampling tube suspended ≈15 cm above the flame tip and diluted by a 6 liter·min^{-1} N_2 carrier gas flow. The excess flow was removed through a critical orifice by a pump to provide the desired sample flow rate. The soot-laden flow was subsequently introduced into a diffusion drier to reduce the RH to <0.5%.

Measurements of soot size distributions, morphology, mixing state, and hygroscopicity were conducted by using a system comprising two DMAs (TSI 3081), an APM analyzer, and a condensation particle counter (TSI 3760A). During an experiment, the polydisperse soot aerosol was brought to charge equilibrium by a polonium-210 bipolar diffusion charger, and particles of a known size were selected from the dry aerosol stream by applying a fixed voltage to the first DMA. This monodisperse flow was exposed to sulfuric acid vapor in a 50-cm-long 3-cm-i.d. reservoir containing 86–96 wt % H_2SO_4 solution at room temperature and then to an elevated-RH environment in a multitube Nafion humidifier (Perma Pure), in which the RH was controlled between 5% and 90%. In the TDMA mode, the change in particle size was measured by scanning the voltage applied to the second DMA. In the DMA–APM mode, the change in the particle mass was measured by stepping the APM voltage at selected rotation speeds. The effective density (ρ_{eff}) and fractal dimension (D_f) of aerosol particles were calculated from measured particle mass (m) and mobility diameter (D_p) according to

$$m \propto D_p^{D_f} \qquad [1]$$

$$\rho_{eff} = \frac{6m}{D_p^3 \pi}. \qquad [2]$$

The vapor concentration of H_2SO_4 in the reservoir was determined by using ion-drift–chemical ionization mass spectrometry (21) and ranged from 10^9 to 10^{10} molecules·cm^{-3}. To suppress evaporation of sulfuric acid from the coated soot particles, the RH was adjusted to 5% after H_2SO_4 exposure in all measurements by adding a small flow of humidified nitrogen a few centimeters downstream of the H_2SO_4 reservoir. Thus, the hygroscopic size and mass growth was referenced to the size and mass ratios at 5% RH. Coating with sulfuric acid resulted only in minor (3–15%) broadening in the TDMA particle-size distributions. The error in RH measurements was <2%.

Cloud activation by soot particles was measured by using a commercial CCN counter (Droplet Measurements Technologies). A DMA was used to select the size and determine the size distribution of soot aerosols. The size-selected particles were then introduced into the CCN counter, and the number concentrations of activated particles were measured at a given supersaturation. The particle size to achieve activation at the selected supersaturation was determined from a plot of the ratios of the concentrations of CCN to aerosols as a function of the aerosol size. Soot aerosols without H_2SO_4 exposure exhibited no activation.

The morphology of soot particles was examined by using a JEOL 2010 TEM, which was operated at an accelerating voltage of 100 kV. Samples of the soot-containing aerosols were collected on Cu TEM grids (200 mesh with amorphous carbon film).

Light extinction and scattering by soot aerosols at 532 nm were measured by using a cavity ring-down spectrometer and a nephelometer (TSI 3563), respectively, interfaced to a DMA–DMA system. Absorption was calculated from the difference between extinction and scattering. A monodisperse sample produced by a single DMA contains larger, multiply charged particles, the presence of which can bias the measured optical properties. Therefore, doubly charged particles selected with the second DMA after recharging the aerosol from the first DMA were used for optical measurements.

1. Intergovernmental Panel on Climate Change (2007) *Intergovernmental Climate Change Report* eds Solomon S, *et al*. (Cambridge Univ Press, Cambridge, UK). http://www.ipcc.ch/ipccreports/ar4-wg1.htm.
2. Penner JE, Eddleman H, Novakov T (1993) Towards the development of a global inventory for black carbon emissions. *Atmos Environ A* 27:1277–1295.
3. Chameides WL, Bergin M (2002) Climate change: Soot takes center stage. *Science* 297:2214–2215.
4. Ackerman AS, *et al*. (2000) Reduction of tropical cloudiness by soot. *Science* 288:1042–1047.
5. Jacobson MZ (2001) Strong radiative heating due to the mixing state of black carbon in atmospheric aerosols. *Nature* 409:695–697.
6. McMurry PH, Shepherd M, Vickery J (2004) *Particulate Matter Science for Policy Makers: A NARSTO Assessment* (Cambridge Univ Press, Cambridge, UK).
7. Zhang D, Zhang R (2005) Laboratory investigation of heterogeneous interaction of sulfuric acid with soot. *Environ Sci Technol* 39:5722–5728.
8. Wyslouzil BE, *et al*. (1994) Observation of hydration of single, modified carbon aerosols. *Geophys Res Lett* 21:2107–2110.
9. Saathoff H, *et al*. (2003) Coating of soot and $(NH_4)_2SO_4$ particles by ozonolysis products of alpha-pinene. *J Aerosol Sci* 34:1297–1321.
10. Zuberi B, *et al*. (2005) Hydrophilic properties of aged soot. *Geophys Res Lett* 32, L01807, doi:10.1029/2004GL021496.
11. Kotzick R, Niessner R (1999) The effects of aging processes on critical supersaturation ratios of ultrafine carbon aerosols. *Atmos Environ* 33:2669–2677.
12. Kotzick R, Panne U, Niessner R (1997) Changes in condensation properties of ultrafine carbon particles subjected to oxidation by ozone. *J Aerosol Sci* 28:725–735.
13. Jacobson MZ (2000) A physically-based treatment of elemental carbon optics: Implications for global direct forcing of aerosols. *Geophys Res Lett* 27:217–220.
14. Ramanathan V, Carmichael G (2008) *Nat GeoSci* 1:221–227.
15. Crouzet Y, Marlow WH (1995) Calculations of the equilibrium vapour-pressure of water over adhering 50–200 nm spheres. *Aerosol Sci Technol* 22:43–59.
16. Popovitcheva OB, Trukhin ME, Persiantseva NM, Shonija NK (2001) Water adsorption on aircraft-combustor soot under young plume conditions. *Atmos Environ* 35:1673–1676.
17. Gysel M, *et al*. (2003) Properties of jet engine combustion particles during the PartEmis experiment: Hygroscopic growth at supersaturated conditions. *Geophys Res Lett* 30, doi:10.1029/2003GL017294.
18. Weingartner E, Burtscher H, Baltensperger U (1997) Hygroscopic properties of carbon and diesel soot particles. *Atmos Environ* 31:2311–2327.
19. Schnaiter M, *et al*. (2005) Absorption amplification of black carbon internally mixed with secondary organic aerosol. *J Geophys Res* 110, D19204, doi:10.1029/2005JD006046.
20. Mikhailov EF, *et al*. (2006) Optical properties of soot–water drop agglomerates: An experimental study. *J Geophys Res* 111, D07209, doi:10.1029/2005JD006389.
21. Zhang R, *et al*. (2004) Atmospheric new particle formation enhanced by organic acids. *Science* 304:1487–1490.
22. Park K, Cao F, Kittelson DB, McMurry PH (2003) Relationship between particle mass and mobility for diesel exhaust particles. *Environ Sci Technol* 37:577–583.
23. Olfert JS, Symonds JPR, Collings N (2007) The effective density and fractal dimension of particles emitted from a light-duty diesel vehicle with a diesel oxidation catalyst. *J Aerosol Sci* 38:69–82.
24. Zhang R, Wooldridge PJ, Abbatt JPD, Molina MJ (1993) Physical chemistry of the H_2SO_4/H_2O binary system at low temperatures: Implications for the stratosphere. *J Phys Chem* 97:7351–7358.
25. Zhang R, Wooldridge PJ, Molina MJ (1993) Vapor pressure measurements for the $H_2SO_4/HNO_3/H_2O$ and $H_2SO_4/HCl/H_2O$ systems: Incorporation of stratospheric acids into background sulfate aerosols. *J Phys Chem* 97:8541–8548.
26. Weber RJ, *et al*. (1997) Measurements of new particle formation and ultrafine particle growth rates at a clean continental site. *J Geophys Res* 102:4375–4385.
27. Eisele FL, McMurry PH (1997) Recent progress in understanding particle nucleation and growth. *Philos Trans R Soc London Ser B* 352:191–201.
28. Hasegawa S, Ohta S (2002) Some measurements of the mixing state of soot-containing particles at urban and non-urban sites. *Atmos Environ* 36:3899–3908.
29. Posfai M, Anderson JR, Buseck PR, Sievering H (1999) Soot and sulfate aerosol particles in the remote marine troposphere. *J Geophys Res* 104:21685–21693.
30. Levitt NP, Zhang R, Xue H, Chen J (2007) Heterogeneous reactions of methylglyoxal in acidic media: Implications for secondary organic aerosol formation. *J Phys Chem A* 111:4804–4814.
31. Zhao J, Levitt NP, Zhang R (2005) Heterogeneous chemistry of octanal and 2,4-hexadienal with sulfuric acid. *Geophys Res Lett* 32, L09802, doi:10.1029/2004GL022200.
32. Levitt NP, Zhao J, Zhang R (2006) Heterogeneous chemistry of butanol and decanol with sulfuric acid: Implications for secondary organic aerosol formation. *J Phys Chem A* 110:13215–13220.
33. Pruppacher HR, Klett JD (1997) *Microphysics of Clouds and Precipitation* (Springer, New York).
34. Fuller KA, Malm WC, Kreidenweis SM (1999) Effects of mixing on extinction by carbonaceous particles. *J Geophys Res* 104:15941–15954.
35. Boubel RW, *et al*. (1994) *Fundamentals of Air Pollution* (Academic, San Diego).
36. Fan F, Zhang R, Tao W-K, Mohr K (2008) Effects of aerosol optical properties on deep convective clouds and radiative forcing. *J Geophys Res* 113, D08209, doi:10.1029/2007JD009257.
37. Zhang R, *et al*. (2007) Intensification of Pacific storm track linked to Asian pollution. *Proc Natl Acad Sci USA* 104:5295–5299.